Large-scale Design Optimization of an Axial-flux Vernier Machine with Dual Stator and Spoke PM Rotor for EV In-wheel Traction

Ali Mohammadi, *Graduate Student Member, IEEE*, Yaser Chulaee, *Graduate Student Member, IEEE*, Aaron M. Cramer, *Senior Member, IEEE*, Ion G. Boldea, *Life Fellow, IEEE*, and Dan M. Ionel, *Fellow, IEEE*

***Abstract*—This paper presents the optimization study targeting a specific drive cycle for a MAGNUS-type axial-flux permanent magnet vernier machine (AFPMVM). The proposed MAGNUS machine has a novel design with a dual-stator configuration, where only one stator is wound, with a high-polarity spoke permanent magnet (PM) rotor. The machine topology has a 3D flux path, which necessitates the analysis of a large finite element (FE) model. However, due to the computational complexity and time required for such a large FE model, a new approach was developed. This approach involves a computationally efficient finite element analysis (CE-FEA) model combined with a single-point drive cycle analysis and the differential evolution (DE) optimization algorithm. The targets of the optimization algorithm are derived by modeling the load operating cycle through a systematic k-means clustering method, identifying specific operating points representing high-energy zones within the drive cycle. The optimized design achieves a wide range of constant power operation, which is desirable for electric vehicle (EV) in-wheel traction. Experimental and numerical results demonstrate a higher torque density in the MAGNUS machine compared to commercially available electric vehicle traction motors. Additionally, the paper explores various flux-weakening methods for the MAGNUS machine, highlighting their respective benefits.**

***Index Terms*—Axial-flux vernier machine, spoke rotor, PM motor, finite element analysis, flux weakening, drive-cycle, electric vehicles, in-wheel traction, differential evolution optimization.**

NOMENCLATURE

β	Torque angle
$\boldsymbol{\lambda}$	Flux linkage
$\boldsymbol{I}$	Current
$\boldsymbol{V}$	Voltage
λ_d	Direct axis flux linkage
λ_{PM}	PM flux linkage
λ_q	Quadrature axis flux linkage
μ_i	Centroid of each cluster
ω	Angular speed
τ_p	Rotor pole pitch
ξ	Saliency ratio
ζ	Flux concentration ratio
C_t	Cost of active materials
D_r	Rotor diameter
F	Clustering objective function
F_1, F_2, F_3	Optimization objectives
h_{PM}	Axial length of the PM
I_d	Direct axis current
I_q	Quadrature axis current
k	Number of clusters
L_d	Direct axis inductance
L_q	Quadrature axis inductance
m_{Cu}	Mass of copper
m_{Fe}	Mass of laminated steel
m_{PM}	Mass of permanent magnets
n_i	Number of data points in each cluster
n_{PM}	Number of permanent magnets
P_ℓ	Sum of copper and core losses
r_s	Resistance
t_a	Number of active stator teeth
t_i	Integer except for multiples of 3
t_p	Number of passive stator teeth
V_d	Direct axis voltage
V_q	Quadrature axis voltage
x_i	Data points of drive cycle
T_{avg}	Average electromagnetic torque
T_{em}	Electromagnetic torque
T_{max}	Maximum electromagnetic torque
T_{min}	Minimum electromagnetic torque
AFPM	Axial-flux permanent magnet
AFPMVM	Axial-flux permanent magnet vernier machine
CE	Computationally efficient
d-axis	Direct axis
DE	Differential evolution
EV	Electric vehicle
FEA	Finite element analysis
GHz	Gigahertz
HEV	Hybrid electric vehicle
IM	Induction machine
IPM	Interior permanent magnet
PM	Permanent magnet
PMSM	Permanent magnet synchronous machine
q-axis	Quadrature axis

I. INTRODUCTION

The ongoing electrification of transportation is a transformative shift in the automotive industry and great emphasis has been dedicated to development of electric vehicles and hybrid electric vehicles (HEVs). In a recent study, Fahimi *et al.* forecast about 20% annual growth from 2023 to 2030 in the EV motor deployment [1], which is attributed to key factors

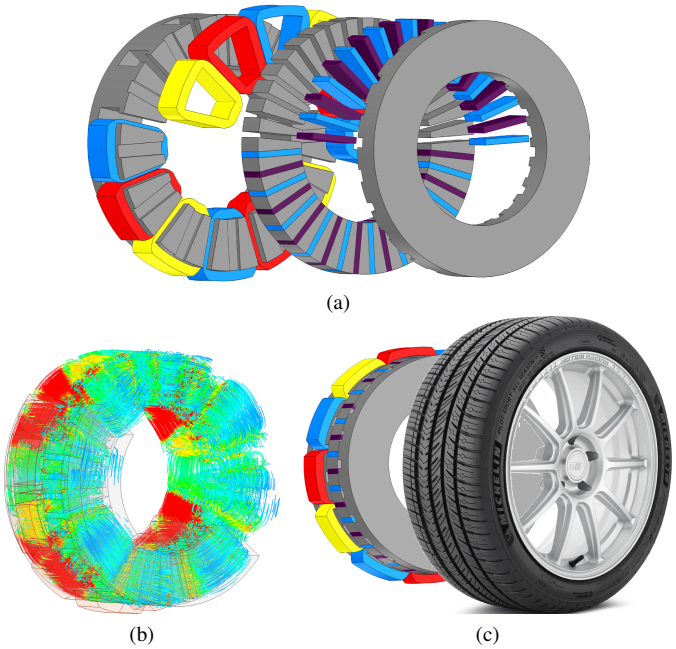

Fig. 1. The electric motor topology for in-wheel traction. (a) Exploded view of the MAGNUS machine with double stators and the rotor with PMs in the middle. (b) The flux density distribution of the machine at the rated loading. (c) The in-wheel schematic to demonstrate the integration of the electric motor and the vehicle wheel.

such as high efficiency and compact design contributing to the recent developments.

As the demand for EVs and HEVs continues to grow, the development of direct-drive electric machines has emerged as an important area of research. A recent literature review on the direct drive electric machines reported by Cai *et al.* included vernier machines and examined their design considerations and performance [2]. Vernier machines as described by Rallabandi *et al.*, have shown promise particularly for low-speed direct-drive applications [3], and emphasis on optimizing the design of these electric machines considering specific drive cycles, is crucial to ensure their optimal performance in EV applications.

This paper, following a brief technology review in Section II, extends the previous work by Mohammadi *et al.* [4], where the design and optimization of an AFPMVM for EV in-wheel traction has been performed. The electromagnetic 3D-FEA as described by Rosu *et al.* is employed [5] and minimum solving time and number of solutions are achieved through modeling a representative symmetric segment of the motor geometry, and utilization of CE-FEA as described in Section III. The analysis of the drive cycle and the process of selecting optimization objectives are addressed in Section IV. Section V focuses on the study of the in-wheel model optimization setup for traction application. The optimization results and investigation of constant power operation for the selected design are presented in Section VI, and Section VII provides further discussions on the demagnetization avoidance, flux weakening methods and axial forces. Finally, the main findings and conclusions of this paper are summarized in Section VIII.

II. Brief Technology Review

In-wheel electric motor configurations offer advantages for EV applications. This section examines various aspects of in-wheel motors that have been researched, including different machine types, topologies for high torque density, methods for constant power operation, and their respective benefits. Using in-wheel configurations provide advantages when implemented in EVs, for example, Sun *et al.* reported that using four independently-driven motors reduces the mechanical losses associated with the transmission, and therefore increases the efficiency [6].

For traction application, different types of electric machine configurations have been investigated considering specific purposes. For applications requiring flux weakening, Ionel *et al.* derived closed-form equations directly linking the main dimensions including PM length and width to the ideal flux-weakening condition and the rated torque [7]. Wang *et al.* studied the optimization of synchronous reluctance machines [8], and Libbos *et al.* researched the implementation of induction motors [9]. Rallabandi *et al.* explored switched reluctance motors [10], and Sayed *et al.* focused on permanent magnet synchronous machines (PMSMs) [11].

In addition to different electric machine topologies, electric motors with high specific torque have been a major subject of ongoing research. Ionel *et al.* proposed an interior PM (IPM) machine with flux barriers in the q-axis, which can produce more torque in comparison to conventional IPM machines [12]. Axial-flux PM (AFPM) and radial flux spoke-type PM motors were investigated by Mohammadi *et al.* [4] and Fatemi *et al.* [13], respectively. Coreless axial-flux PM machines were studied by Chulaee *et al.* [14], and a PM-assisted synchronous reluctance motors were examined by Mohammadi *et al.* [15]. Cai *et al.* reviewed vernier machines and it was reported that in these machines the power factor is inherently low whereas the volumetric torque density can be very high [2].

Among the high torque density topologies studied, machines of the spoke type in axial and radial-flux configurations have been considered by other authors to be particularly suitable for direct-drive applications [16]–[20]. The advantages of spoke-type motors as described by researchers include high rotor polarities that provide opportunities for magnetic flux concentration featuring a very low number of stator coils, which simplifies the manufacturing of stator windings [21]–[25]. While high torque density is crucial for traction motors, an important requirement is constant power operation at speeds above rated speed. Various methods for constant power operation have been explored, as demonstrated by Lawhorn *et al.* [26] where a coreless axial-flux PM synchronous machine, was studied and two novel methods, namely current weakening and relative winding rotation have been proposed.

For high torque density electric motors in EVs, efficient cooling systems are crucial for maintaining optimal temperatures, ensuring long-term reliability and performance. In this paper the MAGNUS type vernier machine has the ability to use single and double-layer coils in slots, which allows

(a)

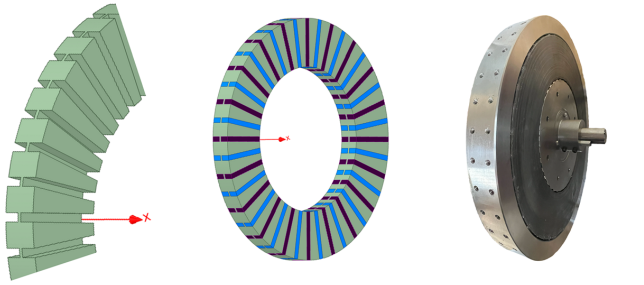

(b)

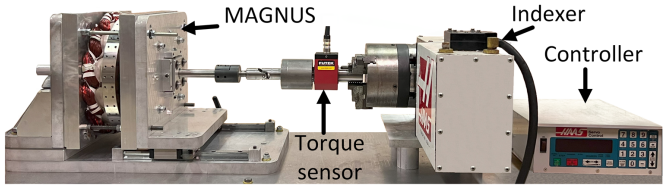

(c)

Fig. 2. (a) The stator has a double-layer winding layout and was fabricated by using a sacrificial aluminum case to protect the laminated core during the machining process. (b) The rotor was made by machining the slots and inserting the 40 PMs in a spoke configuration. (c) The assembly of the vernier machine of the MAGNUS type prototype on the test bench coupled through a torque sensor to an indexer.

for the implementation of advanced cooling systems for improved thermal management. Recent studies considering cooling include for example optimization of various IPM motor designs with different cooling systems by Fatemi *et al.* [27], and demonstration of effective liquid coolant circulation and advanced thermal management strategies by Liu *et al.* [28]. For applications requiring high torque densities, such as in EV traction, effective cooling designs have been shown to be crucial by Jones-Jackson *et al.* [29], and Zaher *et al.* [30] emphasized the importance of cooling in ventilated-type axial-flux PM machines.

III. Motor Topology, Operating Principle, and Computationally Efficient-FEA Model

The innovative configuration of the vernier machine under study comprises two stators – the active and passive stators, each featuring 12 teeth and split poles, as illustrated in Fig. 1(a). The active stator as shown in Fig. 2(a) has 3 phases and 12 coils wound on the main teeth in a double-layer

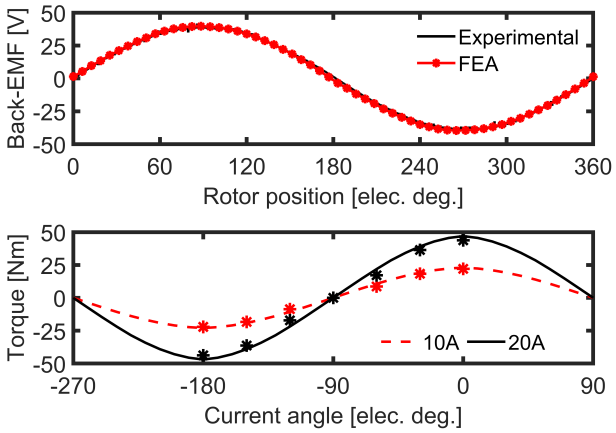

Fig. 3. The comparison between the results from 3D-FEA and experimental tests conducted on the prototype. The open-circuit back-EMF is shown at the top and the static torque is at the bottom. The close agreement of the results validates the computational model.

TABLE I
Possible arrangements of active and passive stators main teeth, auxiliary teeth, and rotor pole counts for three-phase vernier machines.

Main teeth	Armature poles	Auxiliary teeth	Rotor poles
6	4	2 3 4	20 32 44
9	6	2 3 4	30 48 66
12	8	2 3 4	40 64 88
18	12	2 3 4	60 96 132

arrangement, while the passive stator is profiled similarly to the active stator but without any coils in its slots.

To enhance flux concentration and minimize flux leakage, the two stators are rotated relative to each other by 1 rotor pole pitch, as discussed in [31]. In one implementation of the MAGNUS machine suitable for in-wheel traction, given that the passive stator has no coils, it can be integrated into the supporting structure as shown in Fig. 1(c). This integration is of special interest in in-wheel traction applications where the envelope is axially limited.

There is a wide range of options for slot-pole combinations that can be used for this machine. To determine the number of rotor poles required for a three-phase machine, two conditions need to be considered. The first condition states that there must be an odd number of PM poles facing each stator tooth to ensure that only PM poles of one polarity contribute to the phase flux linkage at any given time. The second condition requires a phase shift of 120 degrees between the phases [32]. These conditions can be expressed as:

$$P_r > (2t_p - 1)t_a, \tag{1}$$

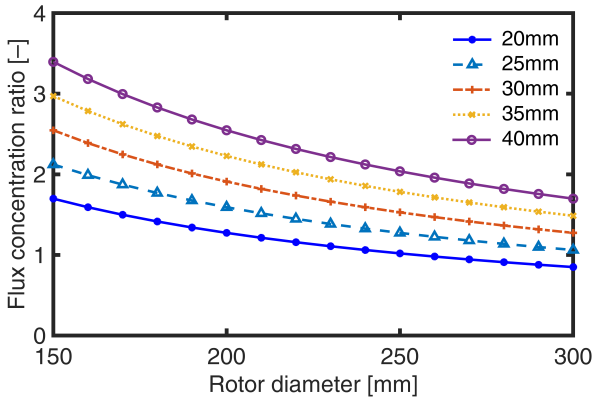

Fig. 4. Flux concentration ratio versus rotor diameter for different rotor axial lengths. The highest to lowest flux concentration ratios are at lower to higher radii, respectively.

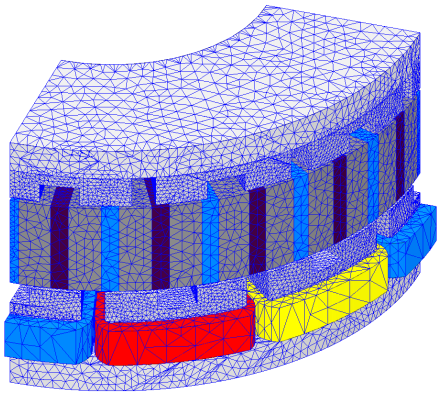

Fig. 5. The 3D computational domain used for analysis shows the tetrahedral mesh elements.

$$P_r = \frac{2}{3} t_a t_i, \tag{2}$$

where t_p is the number of passive stator teeth, P_r represents the number of rotor poles, t_a is the number of active stator teeth, and the value of t_i can be any number except for multiples of 3. In a three-phase vernier machine, feasible combinations of slot-pole are listed in Table I.

The machine under study has 12 teeth with 2 auxiliary teeth on the stator, and 40 rotor poles. For stators, 12 is the minimum number of teeth that allows for series and parallel connections between the coils, which would not be feasible with fewer teeth. Among the different possible rotor polarities, 40 magnetic poles represent the maximum polarity achievable given the prototype's diameter constraints. It should also be noted that previous studies evaluating various slot/poles have indicated that the 12 slots and 40 poles configuration offers the highest efficiency and power factor compared to other combinations [32].

The stator structure of the MAGNUS machine allows for a single-layer coil per slot configuration. In the in-wheel traction setup, illustrated in Fig. 1(c), the machine gains an advantage by being able to provide direct cooling for the active stator winding. This design facilitates having high current density values because of the unique stator structure that enables the implementation of advanced cooling systems, including micro-channels in the middle of the slot.

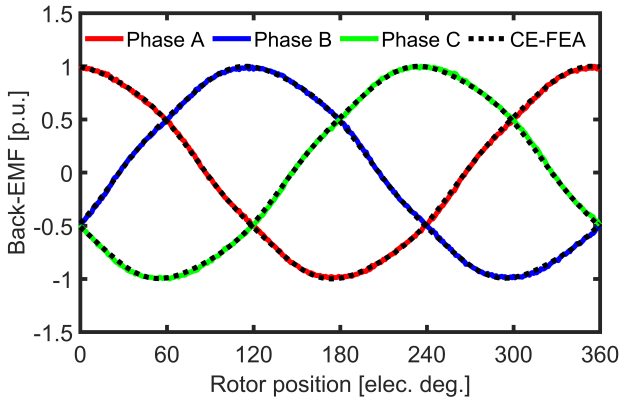

(a)

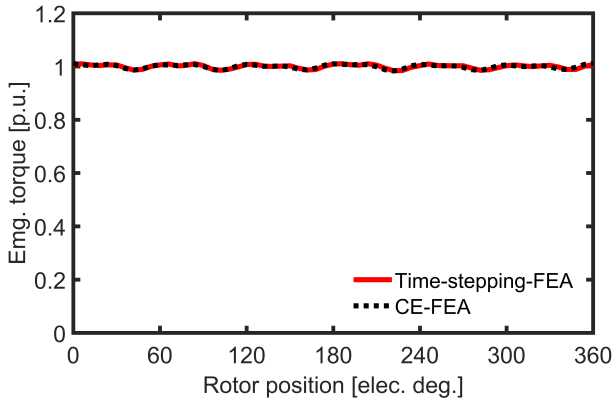

(b)

Fig. 6. The characteristics derived by time-stepping-FEA and computationally efficient FEA, (a) the 3-phase back-EMF of the model at the rated speed of 350rpm, and (b) the electromagnetic torque waveform.

In the MAGNUS machine, as shown in Fig. 2(b) the spoke-type configuration of the rotor incorporates 40 permanent magnets, arranged such that the flux of two adjacent magnets faces each other, leading to a significant concentration of flux. The effect of this high flux concentration can be shown by studying the machine at different conditions. It is worth mentioning that the PM type used in the prototype is NdFeB and the dimension of PMs are approximately $6 \times 30 \times 50$ mm, which were cut and finished with precision to these dimensions.

The flux concentration ratio, ζ, for a double stator axial-flux spoke topology can be defined as:

$$\zeta = \frac{h_{PM}}{\tau_p}, \tag{3}$$

where h_{PM} is the axial length of the permanent magnet, and τ_p is the rotor pole pitch, defined as:

$$\tau_p = \frac{\pi D_r}{n_{PM}}, \tag{4}$$

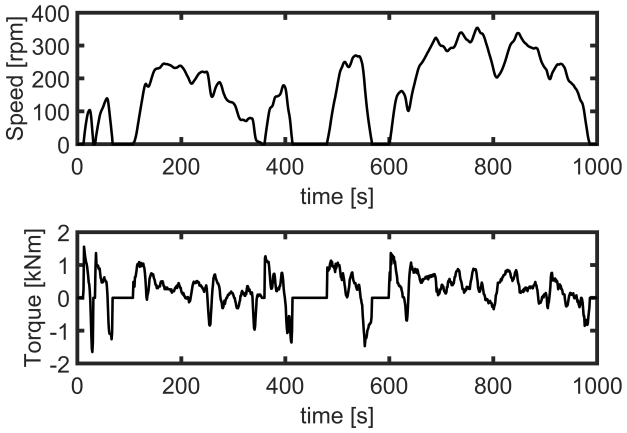

Fig. 7. The electric motor load profile over the WLTP driving cycle where the torque and speed requirements on the cycle are used for the drive cycle analysis.

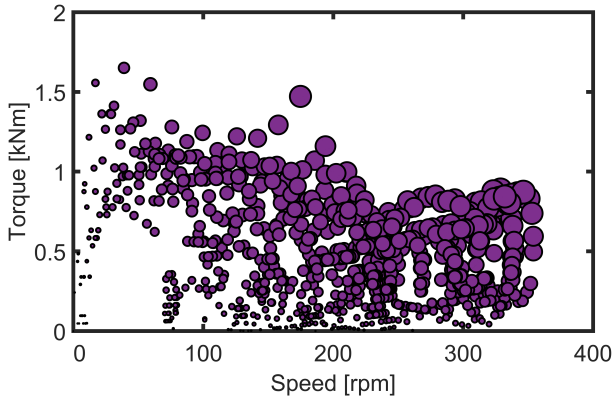

Fig. 8. Distribution of the data points over the WLTP drive-cycle. The size of each circle is proportional to the respective energy use.

where D_r is the rotor diameter, and n_{PM} is the number of permanent magnets. One of the studies specifically performed was to show the flux concentration ratio at different positions in the radial direction in the machine airgap as depicted in Fig. 4. Increasing the rotor axial length directly increases the flux concentration ratio, whereas it decreases as the circumference of the machine increases. In this model, the inner and outer diameters of the rotor are 150 and 300 mm, respectively.

This paper utilizes a vernier machine prototype as a calibrated model for analysis, as demonstrated in Fig. 2(c), which depicts the prototype on the test bench developed for experimental measurements. Using this test bench, the static torque produced by the prototype was measured by the torque sensor at different angles. To accurately measure the static torque, the position of the rotor was precisely controlled by an indexer, which serves as a locking mechanism during the measurements. The results of the experimental tests on the prototype are presented in Fig. 3, where the close agreement between the 3D-FEA and test results verifies the accuracy of the simulated model. This prototype is essential to this paper as it serves as a calibrated model for the design analysis and validation of optimization results.

Solving a time-stepping large FEA model with 3D flux pathways, as shown in Fig. 1(b), is a time-consuming and computationally expensive task. A time-stepping solution refers to solving FE models with a large number of steps in each electric cycle, which can be shortened by modeling a smaller computational domain of the design, illustrated in Fig. 5. The model shown in Fig. 5 requires more than half a million tetrahedral mesh elements and solving a time-stepping 3D-FEA transient analysis for the aforementioned model can take more than six hours, even on a workstation with an AMD Ryzen 3.8-GHz processor with 24 cores.

Despite using a powerful workstation, the run time of each design is not efficient for optimization, therefore the implementation of computationally efficient finite element analysis can be beneficial. Using CE-FEA means solving the 3D-FEA model only for a certain number of steps determined by the Nyquist theorem. According to this theorem to accurately derive a signal, the sampling frequency should be at least twice the frequency of the highest harmonic order in the signal. The electromagnetic torque curve of the MAGNUS machine, depicted in Fig. 6(b), includes the first and sixth-order harmonics. Consequently, the 3D-FEA model requires only 13 FE solutions per electric cycle, accurately deriving the required results approximately 80% faster, thereby saving significant computation time.

The CE-FEA method is advantageous in studying synchronous machines regulated by sine-wave currents, leveraging the inherent symmetries in the electric and magnetic circuits of these machines [33], [34]. Using CE-FEA results in significant computational power savings compared to employing time-stepping 3D-FEA models of the same machines. The accuracy of proposed CE-FEA in this paper is depicted in Fig. 6(a) and Fig. 6(b), which show the 3-phase induced voltages and electromagnetic torque of the MAGNUS machine, respectively. The alignment of the time-stepping and CE-FEA signals demonstrates the efficacy of this method, employed to reduce the computational time of the 3D-FEA simulations used for optimization.

IV. Drive-Cycle Analysis

The drive cycle information includes the operating torque and speed of the electric motor throughout its duration [35]. Depending on the weight of the electric vehicle, multiple specifications for the in-wheel traction motors have been developed. Electric motors with 400 Nm of peak torque and a range of 20 to 40 kW of peak power can be used in lightweight vehicles that can be fully electric vehicles or even hybrid. In-wheel motors developed with 700 Nm of peak torque and 75 kW of peak power are used in heavier vehicles, including passenger cars. For trains and buses, more powerful in-wheel motors have been designed with more than 1,000 Nm of peak torque and 90 kW of peak power [4].

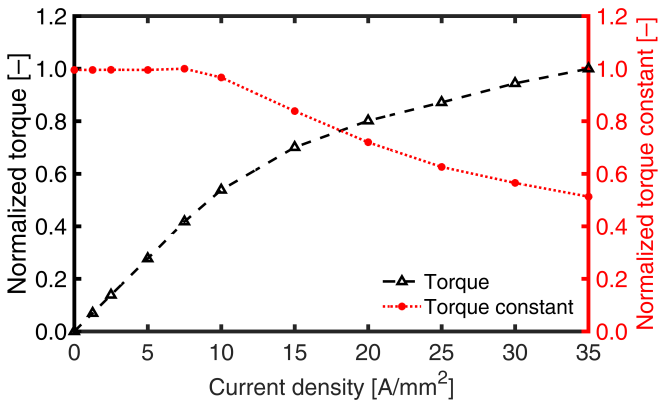

Fig. 9. The normalized electromagnetic torque and torque constant versus current density for the design with 300mm diameter, illustrating also the effect of saturation.

The selected drive cycle in this paper is the Worldwide Harmonised Light Vehicle Test Procedure (WLTP) and its torque and speed requirements are depicted in Fig. 7. The WLTP drive cycle is important in evaluating the performance of electric vehicles, as this harmonized driving cycle, including various driving conditions, serves as a standard for assessing the torque and speed requirements of electric motors. By incorporating the WLTP drive cycle into the optimization process, the potential of electric machines under real-world driving scenarios can be studied [36].

To anticipate distinct patterns and classify the driving conditions within the WLTP drive cycle, the k-means cluster analysis, a powerful machine learning technique can be employed. This method is instrumental in identifying inherent structures and grouping similar data points based on their characteristics [36]. Modeling the load operating cycle using systematic k-means clustering involves collecting and pre-processing data on load parameters, selecting relevant features, initializing the algorithm, and clustering the data into distinct patterns.

Through cluster analysis, characteristic load profiles are identified, and a model is constructed to represent each cluster's behavior. This model can be validated and utilized for load forecasting, energy management, and system optimization, offering meaningful perspectives for efficient operation. Let X represent the features extracted from the WLTP drive cycle dataset to be defined as:

$$X = \{x_1, x_2, ..., x_n\}, \tag{5}$$

where each x_i corresponds to a specific data point. The k-means algorithm seeks to minimize the within-cluster sum of squares, defined by the objective function F as:

$$F = \sum_{i=1}^{k} \sum_{j=1}^{n_i} ||x_{ij} - \mu_i||^2, \tag{6}$$

where k denotes the number of clusters, n_i is the number of data points in cluster i, and μ_i represents the centroid of cluster i.

The iterative process of assigning data points to clusters and updating centroids continuously until convergence yields meaningful groups that each represent distinct driving behavior segments within the WLTP drive cycle. This approach allows for a comprehensive understanding of the electric machine's response to varied driving conditions and contributes valuable insights to the optimization of electric vehicle propulsion systems.

TABLE II
INDEPENDENT VARIABLES FOR THE OPTIMIZATION, THEIR DESCRIPTION BASED ON DESIGN SPECIFICATIONS, AND CORRESPONDING RANGES.

NO	Variable	Dimensional ratio/Length	Min	Max
1	*k_Teeth_l*	Teeth to stator length [–]	0.45	0.80
2	*k_Teeth_w*	Teeth to pole width [–]	0.20	0.40
3	*k_Passive*	Passive to active stator length [–]	0.75	1.45
4	*k_Aux_l*	Aux. teeth to stator length [–]	0.25	0.70
5	*k_Aux_w*	Aux. teeth to pole width [–]	0.50	0.85
6	*k_PM_w*	PM to pole width [–]	0.35	0.90
7	PM_ℓ	PM length [mm]	20.0	50.0
8	$Active_\ell$	Active stator length [mm]	30.0	56.0

Various cluster assumptions may be investigated to analyze the torque and speed characteristics of the electric motor throughout the drive cycle. While considering different cluster numbers, a more refined approach involved treating each point in the drive cycle depicted in Fig. 8 as an individual cluster. Utilizing a weighted average, the torque and speed requirements were determined, considering the energy weight of each data point, which is calculated and normalized by multiplying the required shaft torque and speed of operation at that point. Identifying high energy zones, and calculating their weighted average, resulted in a single representative point for optimization of the electric motor. The resulted torque and speed are 621 Nm and 230 rpm, respectively.

V. Problem Formulation and Differential Evolution Optimization

In the preceding section, the target electromagnetic torque and speed for optimization were determined. In this section, prior to optimization, the prototype model underwent examination across various current density values. The MAGNUS machine, designed specifically for in-slot stator cooling, can operate with a minimal number of coils, enabling a high current density. The normalized electromagnetic torque and torque constant in Fig. 9 are plotted against current density, with the latter corresponding to a slot fill factor of 0.4 for the laboratory prototype. Notably, in manufactured products employing cutting-edge technology, the current density can be significantly reduced, by advancements that allow for an increased slot fill factor of up to 0.7 [37]–[40].

The torque and torque constant curves depicted in Fig. 9 were derived through 3D finite element analysis using ANSYS Electronics software [41]. These curves were normalized based on the 540Nm torque generated by the design, with a consideration for a 50% overload beyond this rated torque. This equates to an overload capability of up to 85 kW of electromagnetic power, showcasing the versatility of the design for a broad spectrum of applications, particularly in-wheel traction.

The proposed concept is for in-wheel direct drive system in which there is no gearbox. In such systems that do not incorporate a gearbox, the electric machine is typically large in size and the cost associated with it dominates the motor-drive system cost. Therefore, the power factor, which impacts the cost of power electronics is less of a concern. In an study on different slot/pole combinations it was shown that in the design with 12 slot and 40 poles power factors as high as 0.75 are possible [32], and in the current optimal design the rated power factor is approximately 0.7. It is also acknowledged that the power factor in vernier machines is inherently low [2] and it is variable with load in PMSMs as shown for example in YASA, (see Fig. 8 in reference [42]).

The model of the MAGNUS-type vernier machine considered for the optimization has an outer diameter of 300 mm, which corresponds to the wheel dimensions in electric vehicles for the WLTP driving cycle, therefore it was considered to be constant during the optimization process. The current density and the number of magnetic poles were also predetermined considering the thermal and operating conditions, respectively, while other geometrical variables were systematically adjusted through the optimization process to target the most favorable design that can satisfy the objectives.

A popular optimization method, which has been implemented in various fields is differential evolution (DE). This population-based optimization method is based on the principle of improving a group of potential solutions over many iterations [43]–[45]. Differential evolution exhibits a balance between exploration and exploitation, ensuring a comprehensive search for the optimal solution without getting stuck in local minima. These attributes, combined with the method's versatility and adaptability, contribute to its effectiveness in achieving the targeted objectives in the optimization processes.

The differential evolution optimization method offers several advantages that make it a popular choice. One key benefit is that this method is known for its robustness and efficiency in handling complex, and nonlinear, optimization problems. Its ability to navigate through solution spaces effectively makes it particularly suitable for electric machine design optimization, where intricate relationships between parameters must be considered during the optimization process.

In traction applications, key objectives include smooth operation, high efficiency, and power density for in-wheel electric motors. Therefore, three concurrent objectives to *minimize* losses (F_1), *minimize* torque ripple (F_2), and *maximize* the electromagnetic torque (F_3) were considered and defined as:

$$\begin{aligned} F_1 &= \min(P_\ell), \\ F_2 &= \min(T_r), \\ F_3 &= \max(T_{em}), \end{aligned} \tag{7}$$

with torque ripple defined as:

$$T_r = \frac{T_{max} - T_{min}}{T_{avg}}, \tag{8}$$

where P_ℓ represents the sum of copper and core losses, T_{em} is the electromagnetic torque, and T_{max}, T_{min}, and T_{avg} are the maximum, minimum and average electromagnetic torque, respectively.

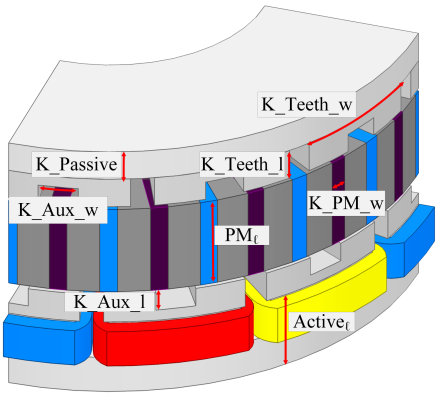

Fig. 10. The independent variables employed for the optimization. The 3D-FEA model corresponds to a quarter of the machine including 10 rotor PMs.

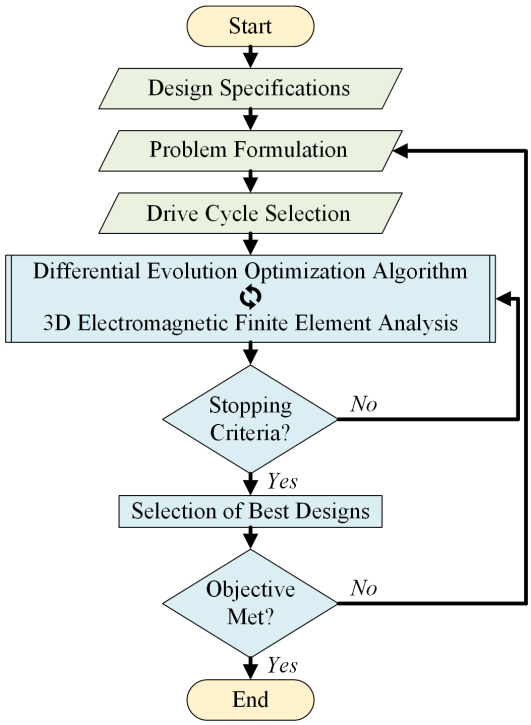

Fig. 11. The flowchart of the proposed optimization process using differential evolution algorithm combined with the single-point drive cycle analysis.

In this paper, eight independent geometrical variables have been considered as shown in Fig. 10, and the variable descriptions and the ranges considered in the optimization process are reported in Table II. The range of independent variables was defined following a sensitivity analysis so that the parametric 3D-FEA simulation model remains robust and the change in the variables keeps the geometrical integrity of the model during the optimization process.

The procedure of the optimization process in Fig. 11, shows each step including the single-point weighted drive cycle analysis which aims to decide the torque and speed requirements of the in-wheel application. The objective of

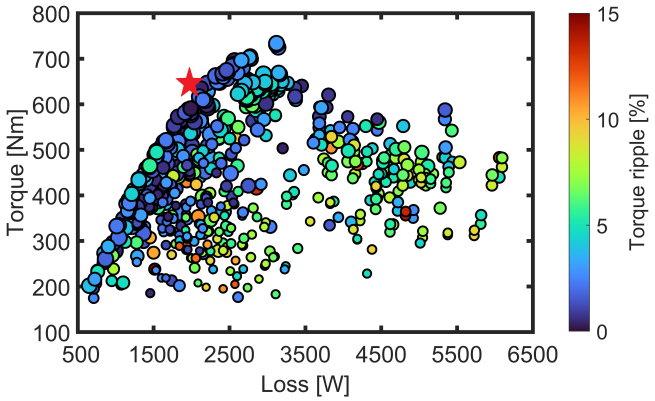

Fig. 12. Results of the differential evolution optimization showing the design distribution considering the torque, loss, and torque ripple. The size of circles indicates their p.u. cost, and the selected design marked with a ★ symbol delivers the required torque while having the relatively lowest cost among the designs on the Pareto.

maximizing the torque provides the possibility of choosing among multiple suitable designs that can deliver the required torque at the designated current density. It is also possible to take advantage of a design that can deliver a higher torque than required by reducing its current density to get the required torque and achieve a higher efficiency for the selected design.

The outer and inner diameters and current density of the model are considered to be constant in the optimization process and the speed of the machine was decided by the drive cycle analysis. The optimization algorithm was scripted in MATLAB software and the process is completely automated, by coupling MATLAB to ANSYS Electronics software. The termination criterion was either a maximum number of generations or a minimal improvement in three representative points of the Pareto front for a few consecutive generations where in this optimization the second criterion was reached.

VI. Optimization Results and Constant Power Operation

In this optimization 750 candidate designs were examined over 15 generations. A population size of 50 designs per generation was considered in the optimization, which was used to ensure an extensive exploration of the design space. The results of the optimization process are depicted in Fig. 12, where the best designs on the Pareto have a very low torque ripple. According to the drive-cycle analysis, the weighted average torque requirement of the WLTP drive cycle is 621Nm, which based on the optimization results the MAGNUS machine can deliver the required torque.

The performance indices of the selected design are reported in Table III, which includes the main geometrical dimensions. The rated speed of the machine is different from the speed considered for the optimization and was considered 350rpm based on the energy weight of the most important data points representative of the drive cycle, considered in the analysis, as shown in Fig. 8.

TABLE III
Specifications of the Proposed Model of the MAGNUS-type Axial-flux PM vernier Machine for In-wheel Traction.

Parameter	Value	Unit
Rated power	30	hp
Rated speed	350	rpm
Peak speed	1,050	rpm
Airgap	1.5	mm
Rotor outer diameter	300	mm
Rotor inner diameter	150	mm
Rated copper losses	2.1	kW
No. of rotor poles	40	–
No. of coils per phase	4	–
No. of turns per phase	104	–
Self inductance	3.2	mH
Mutual inductance	1.5	mH

According to the cost model examples presented by Rosu *et al.* [5], the cost of active materials (C_t) for machines with NdFeB, relative to per unit mass of laminated steel can be estimated by:

$$C_t = 65m_{PM} + 8m_{Cu} + 1m_{Fe}, \tag{9}$$

where m_{Fe} is the mass of laminated steel, m_{Cu} mass of copper, and m_{PM} mass of permanent magnets. By evaluating the cost of active materials and showing the cost by the size of circles in Fig. 12, the selected design shown with a star has the lowest cost amongst the designs on the Pareto front that can deliver the required torque. The selected design has been considered for further analysis for the constant power operation.

In traction applications, a critical aspect of the machine's performance is the torque versus speed curve [12]. The rated characteristics of a PMSM drive with a large flux weakening range has at least two distinct regions. In the initial region, spanning from zero to the base speed, the current is maintained at a constant level, resulting in the motor having a constant torque while the speed increases proportionally to the applied voltage. In the second region, beyond the base speed, both the current and voltage remain constant. However, the torque angle, representing the angle between the PM flux and the armature current, is electronically increased. This adjustment aims to weaken the machine's flux, facilitating an increase in speed at approximately constant power [7].

To maintain the constant power operation, the terminal voltage necessary for running the machine at a specific angular speed ω can be computed as:

$$\begin{aligned} V_d &= r_s I_d - \omega L_q I_q, \\ V_q &= r_s I_q + \omega \lambda_{PM} + \omega L_d I_d, \\ \boldsymbol{V} &= V_d + jV_q, \end{aligned} \tag{10}$$

with the motor current:

$$\boldsymbol{I} = I_d + jI_q, \tag{11}$$

where r_s is the resistance, L_d, the direct (d) axis inductance, L_q, the quadrature (q) axis inductance, V_d, and I_d, the d-axis

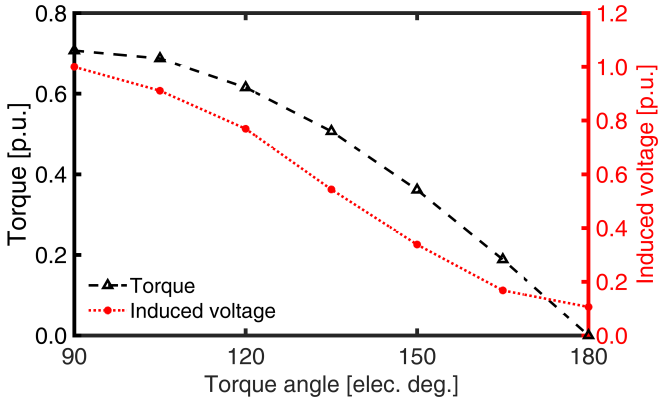

Fig. 13. The electromagnetic torque and per-unit fundamental rms of the induced voltage at the rated current loading and speed versus the torque angle. Owing to non-saliency, the maximum electromagnetic torque is achieved at 90 electric degrees torque angle.

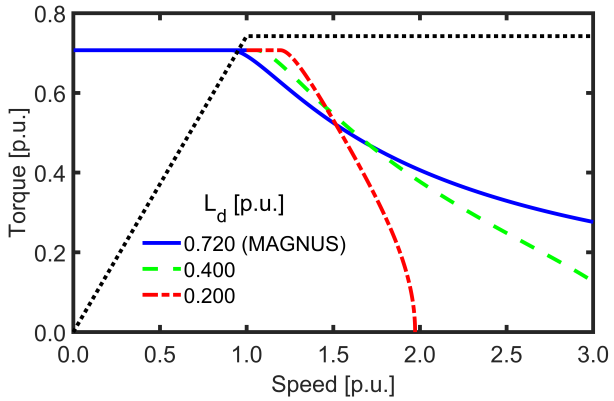

Fig. 14. Torque versus speed characteristics of MAGNUS model and examples of PMSMs with different per-unit d-axis inductances. The MAGNUS motor has a wide constant power operation region as shown with the small-dotted line, which is suitable for EV traction application.

TABLE IV
PERFORMANCE COMPARISON OF THE MAGNUS MACHINE WITH HIGH TORQUE DENSITY TRACTION MOTORS.

Machine (type)	Torque [Nm]	Active mass [kg]	Efficiency [%]	Torque density [Nm/kg]
MAGNUS (AFPM)	625	36	96	17.4
YASA 400 (AFPM)	360	24	95	15.0
Formula E (IPM-spoke)	110	9	96	12.2
Chevrolet Bolt (IPM)	360	33	97	10.9
Honda Accord 14 (IPM)	306	33	94	9.3
Toyota Prius 10 (IPM)	207	23	96	9.0
Tesla Model S (IM)	430	55	98	7.8

voltage and current, V_q, and I_q, the q-axis voltage and current, and λ_{PM} the open-circuit flux linkage.

Assuming no cross-saturation effects (no dq coupling effects), the steady-state dq flux linkages in the synchronous frame of reference can be written as:

$$\begin{aligned} \lambda_d &= \lambda_{PM} + L_d I_d, \\ \lambda_q &= L_q I_q, \\ \boldsymbol{\lambda} &= \lambda_d + j\lambda_q. \end{aligned} \tag{12}$$

The machine's electromagnetic torque can be expressed as:

$$T_{em} = \frac{m}{2}\frac{P}{2}(\boldsymbol{\lambda} \times \boldsymbol{I}) = \frac{m}{2}\frac{P}{2}\left(\lambda_d I_q - \lambda_q I_d\right), \tag{13}$$

where m is the number of phases and P number of poles. Assuming a linear magnetic circuit and neglecting dq cross-saturation effects as implied in Eq. (12), the torque equation can be further expressed in terms of the machine's direct and quadrature axes inductances (L_d and L_q) and the PM flux linking the armature winding (λ_{pm}), as:

$$T_{em} = \frac{3}{2}\frac{P}{2}\left(\lambda_{PM} I_q + \left(L_d - L_q\right) I_d I_q\right) \tag{14}$$

In the MAGNUS machine $L_d \approx L_q$, therefore the machine's saliency ratio (ξ) is approximately 1, hence the reluctance torque is negligible. In a PMSM, where the saliency is 1, to decouple the d- and q-axis components of the current, the rotor reference frame-oriented control is employed. When $\xi = 1$ the maximum torque per ampere (MTPA) is obtained when the d-axis current is driven to zero or the torque angle (β) is maintained at 90 degrees with respect to the q-axis. At higher speeds, a negative I_d can be used to reduce the terminal voltage. The value of I_d is increased such that the total phase current is constant.

The flux linkage reduces with increasing value of negative I_d (i.e. $90^o < \beta < 180^o$) such that the terminal voltage is constant. The torque profile of the machine under study in this research is depicted in Fig. 13; in this model, the saliency ratio is close to one, hence, d and q-axis inductances are almost equal, which can be seen in the electromagnetic torque curve where the maximum electromagnetic torque is at $\beta = 90^o$.

The analytically calculated torque-speed characteristics for different values of per-unit L_d and the dependence of the width of the constant power region on the d-axis inductance values are shown in Fig. 14. Lower values of per-unit inductance, lead to a narrower constant power region. The torque-speed characteristics were calculated assuming an available terminal voltage of 1 p.u. in machines with different values of per-unit inductances.

VII. DISCUSSION

A comparison of the *optimal* design of this paper to high-torque-density traction motors available in the market is presented in Table IV. This comparison relies on the approximate performance of traction motors with high torque density, utilizing information that is publicly accessible [2], [13], [46]–[49]. It should be noted that detailed component active material mass for these machines are not publicly available. The comparison results show that MAGNUS machine demonstrates a superior performance to these advanced commercially available motors in terms of peak torque density and performs with a competitive efficiency.

The MAGNUS motor can operate with 91% efficiency at the rated speed of only 350 rpm and by increasing the speed to the

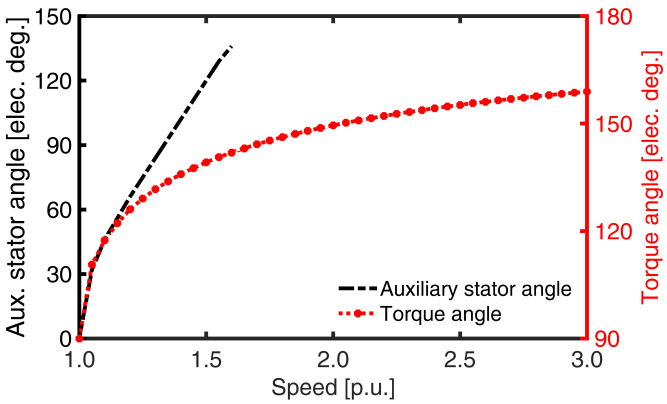

Fig. 15. Flux weakening mechanism by torque angle phase advance and the mechanical rotation of the passive stator with respect to the active stator and the initial position of the rotor, which can result in 40% voltage reduction.

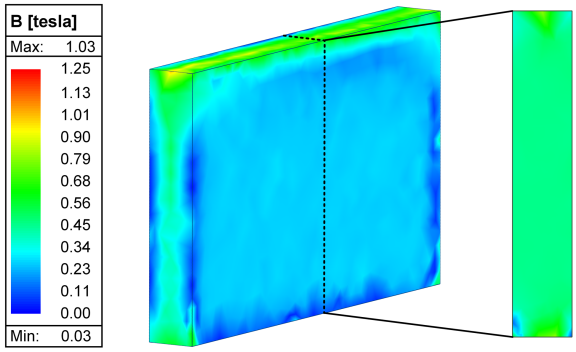

Fig. 16. Demagnetization study by injecting negative d-axis current, which illustrates successful demagnetization avoidance. The PM remanence is 1.25T, and the irreversible demagnetization knee point is 0.075T. The figure is a representation of one PM and its cross-section.

peak of 1,050 rpm the efficiency increases to 96% delivering its peak power. It should be noted that by increasing the slot fill factor from the 40% considered in this paper to 70% and using innovative winding solutions providing a very high slot fill factor as introduced by Marsilli and others [37]–[40], the efficiency of the MAGNUS machine can be further increased.

Flux weakening is a requirement for traction machines, as it allows the machine to operate above the base speed while still maintaining the maximum terminal voltage. The machine under study in this paper has a high per-unit inductance and a wide constant operation region also shown in Fig. 14, while maintaining a constant voltage of 1 p.u. at higher speeds, and is able to perform flux weakening.

In the MAGNUS machine, one approach for flux weakening, in addition to using current phase advance, involves mechanical rotation in the passive stator. Mechanical flux weakening has been previously introduced to maintain constant power for PMSMs as discussed in [17]. It is worth noting that the implementation of this method requires a servo motor with acceleration and stopping times on the order of tens of milliseconds. The passive stator of MAGNUS can be mechanically rotated with respect to the active stator for 9 mechanical degrees (equivalent to 180 electric degrees). By

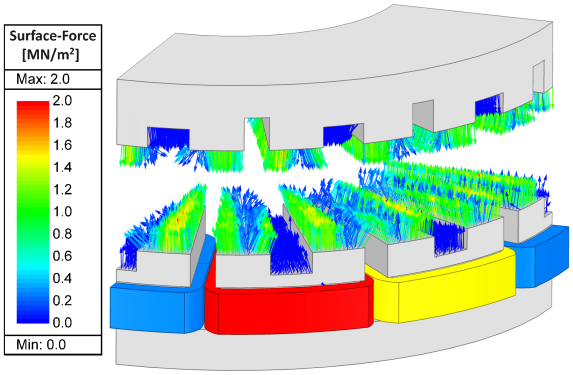

Fig. 17. Study on axial force density of stators shows the surface force distribution calculated with the rotor in between, but for clarity the rotor is not shown. The analysis results indicate the difference between average surface-forces on active and passive stators is less than 3%.

TABLE V
BREAKDOWN OF THE TANGENTIAL AND AXIAL FORCES ON THE STATOR AND ROTOR FOR THE VERNIER MACHINE OF THE MAGNUS TYPE.

Force	Rotor FAS	Rotor FPS	Active stator	Passive stator
Tangential [kN]	3.64	1.82	-3.64	-1.82
Axial [kN]	-18.98	19.14	20.03	-19.48

doing so, as illustrated in Fig. 15, the voltage can be reduced to 60% of its nominal value.

Additional techniques, for instance, dynamic winding reconfiguration, can be employed to further decrease the machine's voltage at higher speeds. As an example, in a particular implementation, the windings can be configured in series to operate within the constant torque region of the torque-speed characteristics, and in parallel for operation within the constant power region. This method contributes to a broader range of operational flexibility, allowing optimal performance across different speeds through strategic winding adjustments.

To ensure reliable operation, demagnetization modeling is conducted. A negative d-axis current, twice the rated current, is employed as the excitation for optimal design at the operating temperature of 100°C. The PM operating point was observed through FEA, and Fig. 16 illustrates that the PM surface facing the teeth experiences no demagnetization. However, negligible demagnetization is observed along the top and bottom edges where the PM faces the stators.

It is important to mention that axial flux permanent magnet machines offer high torque density and compact axial length, but face challenges related to manufacturing complexity due to their unique disk-shaped geometry and multi-air gap construction. Additionally, the extensive use of rare-earth permanent magnets can significantly increase the overall system cost. Among the challenges faced by AFPM machines, the attraction forces between the stators and the rotor can be substantial and require careful analysis.

The distribution of axial surface forces on the stators is depicted in Fig. 17, where the rotor is not shown for a clearer view of the forces. The breakdown of axial and tangential components of forces on stators and the rotor side facing

the active stator (FAS) and the other side facing the passive stator (FPS) are reported in Table V. The average axial forces on the stators and rotor are approximately 20 kN, with a difference of less than 3% between them. This relatively small force imbalance, which can be effectively counteracted by the bearing system design, is owed to the passive stator, which greatly balances the axial forces and also contributes to torque as documented in [22].

VIII. Conclusion

The PM axial-flux vernier-type machine referred to as MAGNUS has been proposed and studied in this paper for in-wheel traction application. The machine has an innovative structure with two stators, reduced number of concentrated coils, a spoke PM rotor with very high polarity. It has a three dimensional flux path, requiring a quarter of the structure to be analyzed by very large 3D FE models. In order to minimize the very high computational effort, new specific methods have been proposed for computational-efficient (CE) electromagnetic FEA, a single-point weighted representative approach for drive-cycle analysis, and differential evolutionary (DE) optimization with hundreds of candidate designs.

Based on a combination of experimental and numerical results, the proposed MAGNUS prototype motor design has a torque density higher than commercially available motors for EVs. Furthermore, this MAGNUS machine can operate with double-layer and single-layer concentrated coils enabling advanced cooling systems for the active stator only. Various innovative flux-weakening methods, such as the mechanical rotation of the passive stator and dynamic winding reconfiguration, may be applied. It was also shown that conventional vector control method for advancing the torque angle is possible for the proposed design, which has a high per-unit d-axis inductance that enables a very wide constant power operation range suitable for EV traction application.

Acknowledgment

This paper is based upon work supported by the National Science Foundation (NSF) under Award No. #1809876. Any opinions, findings, conclusions, or recommendations expressed in this material are those of the authors and do not necessarily reflect the views of the NSF. The support of Ansys Inc., and University of Kentucky the L. Stanley Pigman Chair in Power endowment is also gratefully acknowledged. Special thanks are due to Mr. J. R. Hendershot of Motorsolver LLC, for his design contributions and the fabrication of the prototype motor.

References

[1] B. Fahimi, L. H. Lewis, J. M. Miller, S. D. Pekarek, I. Boldea, B. Ozpineci, K. Hameyer, S. Schulz, A. Ghaderi, M. Popescu, B. Lehman, and D. D. Patel, "Automotive Electric Propulsion Systems: A Technology Outlook," *IEEE Transactions on Transportation Electrification*, vol. 10, pp. 1–28, 2023.

[2] S. Cai, J. L. Kirtley, and C. H. T. Lee, "Critical Review of Direct-Drive Electrical Machine Systems for Electric and Hybrid Electric Vehicles," *IEEE Transactions on Energy Conversion*, vol. 37, no. 4, pp. 2657–2668, 2022.

[3] V. Rallabandi, P. Han, M. G. Kesgin, N. Taran, and D. M. Ionel, "Axial-field Vernier-type Flux Modulation Machines for Low-speed Direct-drive Applications," in *2019 IEEE Energy Conversion Congress and Exposition (ECCE)*, 2019, pp. 3123–3128.

[4] A. Mohammadi, Y. Chulaee, A. M. Cramer, I. Boldea, and D. M. Ionel, "Axial Flux Permanent Magnet Vernier Machine with Single-wound Dual-stator and Spoke Permanent Magnet Rotor for Electric Vehicle In-wheel Traction," in *2023 IEEE Transportation Electrification Conference & Expo (ITEC)*, 2023, pp. 1–5.

[5] M. Rosu, P. Zhou, D. Lin, D. M. Ionel, M. Popescu, F. Blaabjerg, V. Rallabandi, and D. Staton, *Multiphysics Simulation by Design for Electrical Machines, Power Electronics and Drives*. J. Wiley - IEEE Press, 2017, doi: 10.1002/9781119103462.

[6] X. Sun, Z. Shi, Y. Cai, G. Lei, Y. Guo, and J. Zhu, "Driving-Cycle-Oriented Design Optimization of a Permanent Magnet Hub Motor Drive System for a Four-Wheel-Drive Electric Vehicle," *IEEE Transactions on Transportation Electrification*, vol. 6, no. 3, pp. 1115–1125, 2020.

[7] D. M. Ionel, J. F. Eastham, T. Miller, and E. Demeter, "Design considerations for permanent magnet synchronous motors for flux weakening applications," *IEE Proceedings-Electric Power Applications*, vol. 145, no. 5, pp. 435–440, 1998.

[8] Y. Wang, D. M. Ionel, V. Rallabandi, M. Jiang, and S. J. Stretz, "Large-Scale Optimization of Synchronous Reluctance Machines Using CE-FEA and Differential Evolution," *IEEE Transactions on Industry Applications*, vol. 52, no. 6, pp. 4699–4709, 2016.

[9] E. Libbos, E. Krause, A. Banerjee, and P. T. Krein, "Winding Layout Considerations for Variable-Pole Induction Motors in Electric Vehicles," *IEEE Transactions on Transportation Electrification*, pp. 1–1, 2023.

[10] V. Rallabandi, J. Wu, A. M. Cramer, D. M. Ionel, and P. Zhou, "Optimal Design of Outer Rotor Switched Reluctance Machines for Direct Drive Rim Applications," in *2018 IEEE Energy Conversion Congress and Exposition (ECCE)*, 2018, pp. 6104–6109.

[11] E. Sayed, S. M. Castano, J. W. Jiang, J. Liang, G. Pietrini, M. H. Bakr, A. Emadi, and B. Bilgin, "Design of Multilayer Concentric Ferrite-Magnet Machines for a Traction Application," *IEEE Transactions on Transportation Electrification*, vol. 7, no. 3, pp. 1548–1560, 2021.

[12] D. M. Ionel, J. F. Eastham, and T. Betzer, "Finite element analysis of a novel brushless DC motor with flux barriers," *IEEE Transactions on Magnetics*, vol. 31, no. 6, pp. 3749–3751, 1995.

[13] A. Fatemi, D. M. Ionel, M. Popescu, Y. C. Chong, and N. A. O. Demerdash, "Design Optimization of a High Torque Density Spoke-Type PM Motor for a Formula E Race Drive Cycle," *IEEE Transactions on Industry Applications*, vol. 54, no. 5, pp. 4343–4354, 2018.

[14] Y. Chulaee, D. Lewis, A. Mohammadi, G. Heins, D. Patterson, and D. M. Ionel, "Circulating and Eddy Current Losses in Coreless Axial Flux PM Machine Stators With PCB Windings," *IEEE Transactions on Industry Applications*, pp. 1–11, 2023.

[15] A. Mohammadi and S. M. Mirimani, "Design of a novel PM-assisted synchronous reluctance motor topology using V-shape permanent magnets for improvement of torque characteristic," *IEEE Transactions on Energy Conversion*, vol. 37, no. 1, pp. 424–432, 2021.

[16] I. Boldea, L. Tutelea, and M. Topor, "Theoretical characterization of three phase flux reversal machine with rotor-PM flux concentration," in *2012 13th International Conference on Optimization of Electrical and Electronic Equipment (OPTIM)*, 2012, pp. 472–476.

[17] I. Boldea and L. N. Tutelea, "PMSM with rotor PM mechanical flux-weakening (MFW) to zero for an 150kW, 600Vdc, 500–6000 rpm drive: Preliminary design with key validation," in *2016 XXII International Conference on Electrical Machines (ICEM)*, 2016, pp. 1995–2001.

[18] A. Mohammadi, O. A. Badewa, Y. Chulaee, D. D. Lewis, S. Essakiappan, M. Manjrekar, and D. M. Ionel, "Design Optimization of a Direct-Drive Wind Generator With a Reluctance Rotor and a Flux Intensifying Stator Using Different PM Types," *IEEE Transactions on Industry Applications*, pp. 1–10, 2024.

[19] F. Zhao, T. A. Lipo, and B.-I. Kwon, "A Novel Dual-Stator Axial-Flux Spoke-Type Permanent Magnet Vernier Machine for Direct-Drive Applications," *IEEE Transactions on Magnetics*, vol. 50, no. 11, pp. 1–4, 2014.

[20] A. Mohammadi, O. A. Badewa, Y. Chulaee, D. M. Ionel, S. Essakiappan, and M. Manjrekar, "Direct-Drive Wind Generator Concept with Non-Rare-Earth PM Flux Intensifying Stator and Reluctance Outer Rotor," in *2022 11th International Conference on Renewable Energy Research and Application (ICRERA)*. IEEE, 2022, pp. 582–587.

[21] A. Mohammadi, Y. Chulaee, A. M. Cramer, I. Boldea, and D. M. Ionel, "Parameter identification, non-linearity, and harmonic effects in a vernier machine of the magnus type," in *2023 IEEE Energy Conversion Congress and Exposition (ECCE)*, 2023, pp. 4286–4291.

[22] M. G. Kesgin, P. Han, D. Lawhorn, and D. M. Ionel, "Analysis of Torque Production in Axial-flux Vernier PM Machines of the MAGNUS Type," in *2021 IEEE International Electric Machines & Drives Conference (IEMDC)*, 2021, pp. 1–5.

[23] G. Heins, D. M. Ionel, and M. Thiele, "Winding factors and magnetic fields in permanent magnet brushless machines with concentrated windings and modular stator cores," in *2013 IEEE Energy Conversion Congress and Exposition*, 2013, pp. 5048–5055.

[24] R. Zhang, J. Li, R. Qu, and D. Li, "Analysis and Design of Triple-Rotor Axial-Flux Spoke-Array Vernier Permanent Magnet Machines," *IEEE Transactions on Industry Applications*, vol. 54, no. 1, pp. 244–253, 2018.

[25] A. Mohammadi and S. M. Mirimani, "Design and Analysis of a Novel Permanent Magnet Assisted Synchronous Reluctance Machine Using Finite-Element-Method," in *2020 11th Power Electronics, Drive Systems, and Technologies Conference (PEDSTC)*, 2020, pp. 1–5.

[26] D. Lawhorn, N. Taran, V. Rallabandi, and D. M. Ionel, "A Comparative Study of Constant Power Operation Techniques for Low Inductance Machines," in *2018 IEEE Transportation Electrification Conference and Expo (ITEC)*, 2018, pp. 638–643.

[27] A. Fatemi, D. M. Ionel, N. A. O. Demerdash, and T. W. Nehl, "Optimal Design of IPM Motors With Different Cooling Systems and Winding Configurations," *IEEE Transactions on Industry Applications*, vol. 52, no. 4, pp. 3041–3049, 2016.

[28] F. Liu and X. Wang, "Design and Multiobjective Optimization of Dual-Circulation Cooling System Considering Electro-Thermal Coupling for IPMSM," *IEEE Transactions on Transportation Electrification*, vol. 9, no. 2, pp. 3072–3084, 2023.

[29] S. Jones-Jackson, R. Rodriguez, E. Sayed, C. Goldstein, C. Mak, A. Callegaro, M. Goykhman, and A. Emadi, "Design and Analysis of Stator Cooling Channels for an Axial-Flux Permanent Magnet Machine," in *2021 IEEE Transportation Electrification Conference and Expo (ITEC)*, 2021, pp. 272–277.

[30] I. Zaher, R. Rodriguez, E. Sayed, A. Callegaro, M. Goykhman, and A. Emadi, "Effect of Rotor Geometry on Rotor Air Cooling of a Ventilated Axial-Flux Permanent Magnet Machine," in *2021 IEEE Transportation Electrification Conference and Expo (ITEC)*, 2021, pp. 77–82.

[31] V. Rallabandi, N. Taran, D. M. Ionel, and I. G. Boldea, "Axial-flux PM synchronous machines with air-gap profiling and very high ratio of spoke rotor poles to stator concentrated coils," in *2017 IEEE International Electric Machines and Drives Conference (IEMDC)*, 2017, pp. 1–7.

[32] V. Rallabandi, N. Taran, D. M. Ionel, and I. Boldea, "MAGNUS — An ultra-high specific torque PM axial flux type motor with flux focusing and modulation," in *2017 IEEE Energy Conversion Congress and Exposition (ECCE)*, 2017, pp. 1234–1239.

[33] D. M. Ionel and M. Popescu, "Finite-Element Surrogate Model for Electric Machines With Revolving Field—Application to IPM Motors," *IEEE Transactions on Industry Applications*, vol. 46, no. 6, pp. 2424–2433, 2010.

[34] Y. Chulaee and D. M. Ionel, "Ultra-fast finite element analysis of coreless axial flux permanent magnet synchronous machines," *IET Electric Power Applications*, vol. 18, 2024. [Online]. Available: https://ietresearch.onlinelibrary.wiley.com/doi/abs/10.1049/elp2.12439

[35] A. Fatemi, N. A. O. Demerdash, T. W. Nehl, and D. M. Ionel, "Large-Scale Design Optimization of PM Machines Over a Target Operating Cycle," *IEEE Transactions on Industry Applications*, vol. 52, no. 5, pp. 3772–3782, 2016.

[36] M. Salameh, I. P. Brown, and M. Krishnamurthy, "Fundamental Evaluation of Data Clustering Approaches for Driving Cycle-Based Machine Design Optimization," *IEEE Transactions on Transportation Electrification*, vol. 5, no. 4, pp. 1395–1405, 2019.

[37] Marsilli, *Distributed High Density stator winding*, 2024, accessed February 2024. [Online]. Available: https://marsilli.com/innovations.

[38] J.-W. Chin, K.-S. Cha, M.-R. Park, S.-H. Park, E.-C. Lee, and M.-S. Lim, "High Efficiency PMSM With High Slot Fill Factor Coil for Heavy-Duty EV Traction Considering AC Resistance," *IEEE Transactions on Energy Conversion*, vol. 36, no. 2, pp. 883–894, 2021.

[39] Y. Yang, X. Huang, and J. Fu, "Design and Performance Analysis of Additively Manufactured Windings with High Slot Fill Factor for Permanent Magnet Synchronous Motors," in *2023 26th International Conference on Electrical Machines and Systems (ICEMS)*, 2023, pp. 1384–1389.

[40] A. Dannier, F. Di Bruno, F. Fiume, E. Fedele, and G. Brando, "Hairpin Winding Technology for Electric Traction Motors: Design, Prototyping, and Connection Rules," in *2022 International Conference on Electrical Machines (ICEM)*, 2022, pp. 1170–1175.

[41] *Ansys® Electronics Desktop,, version 23.2, 2023, ANSYS Inc.*

[42] A. Allca-Pekarovic, P. J. Kollmeyer, A. Forsyth, and A. Emadi, "Experimental Characterization and Modeling of a YASA P400 Axial Flux PM Traction Machine for Performance Analysis of a Chevy Bolt EV," *IEEE Transactions on Industry Applications*, vol. 60, no. 2, pp. 3108–3119, 2024.

[43] Y. Duan and D. M. Ionel, "A Review of Recent Developments in Electrical Machine Design Optimization Methods With a Permanent-Magnet Synchronous Motor Benchmark Study," *IEEE Transactions on Industry Applications*, vol. 49, no. 3, pp. 1268–1275, 2013.

[44] R. Storn and K. Price, "Differential Evolution – A Simple and Efficient Heuristic for global Optimization over Continuous Spaces," in *Journal of Global Optimization*, vol. 11, 1997, pp. 341–359.

[45] O. A. Badewa, A. Mohammadi, D. D. Lewis, D. M. Ionel, S. Essakiappan, and M. Manjrekar, "Optimization of an Electric Vehicle Traction Motor with a PM Flux Intensifying Stator and a Reluctance Outer Rotor," in *2023 IEEE Transportation Electrification Conference & Expo (ITEC)*, 2023, pp. 1–6.

[46] F. Momen, K. Rahman, and Y. Son, "Electrical propulsion system design of chevrolet bolt battery electric vehicle," *IEEE Transactions on Industry Applications*, vol. 55, no. 1, pp. 376–384, 2019.

[47] YASA Motors Limited, *YASA-400 Product Sheet*, Oxford, England, 2015, accessed May 2024. [Online]. Available: https://www.e-kart.fr/images/stories/technique/yasa/YASA-400-Product-Sheet.pdf

[48] M. Olszewski, "Evaluation of the 2010 Toyota Prius Hybrid Synergy Drive System," Oak Ridge National Laboratory (ORNL), U.S. Department of Energy, Washington, D.C., United States, Tech. Rep., 2011.

[49] B. Ozpineci, "Oak Ridge National Laboratory annual progress report for the electric drive technologies program (No. ORNL/SPR-2015/626)," Oak Ridge National Lab (ORNL), Oak Ridge, TN, United States, Tech. Rep., 2015.

Ali Mohammadi (Graduate Student Member, IEEE) received the B.Sc. and M.Sc. degrees from the Babol Noshirvani University of Technology (BNUT), Babol, Iran. He is currently working toward the Ph.D. degree with SPARK Laboratory, Department of Electrical and Computer Engineering, University of Kentucky, Lexington, KY, USA. He was the recipient of the Best Paper Award as first author at the 2022 IEEE International Conference on Renewable Energy Research and Applications (ICRERA), the Best Student Paper Award as first author at the 2023 IEEE Transportation Electrification Conference (ITEC), and the First Best Paper Award as a co-author at the 2023 IEEE International Conference on Renewable Energy Research and Applications (ICRERA) all on topics of specialty electric machines. His research focuses on renewable energies, electrification of transportation, advanced electromagnetic FEA, the design and optimization of electric machines, motor drives and power electronics.

Yaser Chulaee (Graduate Student Member, IEEE) received the B.Sc. degree in electrical engineering from the Shahrood University of Technology, Shahrood, Iran, in 2016, and the M.Sc. degree in electrical engineering from the Ferdowsi University of Mashhad, Mashhad, Iran, in 2019. He is currently working toward the Ph.D. degree with SPARK Laboratory, Department of Electrical and Computer Engineering, University of Kentucky, Lexington, KY, USA. His research focuses on advanced electromagnetic FEA, the design and optimization of electric machines, and motor drive systems. He was the recipient of a best paper award as a co-author at the 2022 IEEE International Conference on Renewable Energy Research and Applications (ICRERA), a best paper award as a co-author at the 2023 IEEE Transportation Electrification Conference (ITEC 2023), and a prize paper by the Electric Machines Committee of the IEEE Industrial Applications Society for a paper presented at the 2022 Energy Conversion Conference and Exposition (ECCE 2022).

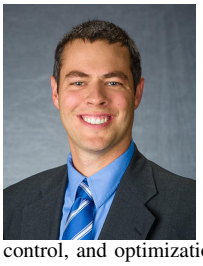

Aaron M. Cramer (Senior Member, IEEE) received the B.S. degree (summa cum laude) in electrical engineering from the University of Kentucky, Lexington, KY, USA, in 2003, and the Ph.D. degree in electrical engineering from Purdue University, West Lafayette, IN, USA, in 2007.,From 2007 to 2010, he was a Senior Engineer with PC Krause and Associates, West Lafayette. In 2010, he joined the University of Kentucky, where he is currently a Professor. His research interests include simulation, control, and optimization of power and energy systems.

Ion Boldea (Life Fellow, IEEE) received the M.S. and Ph.D. degrees in electrical engineering from the University Politehnica of Timisoara, Timisoara, Romania, in 1967 and 1973, respectively.,He is currently a Full Professor with the University Politehnica of Timisoara, Timisoara, Romania. He has authored or coauthored research papers extensively (291 papers, 5395 citations, H index: 40 in Web of Science) in linear and rotary electric machines, drives, and MAGLEVs, and numerous books, with 6000 entrances in libraries worldwide (WorldCat.com)., Dr. Boldea was the recipient of the 2015 IEEE Nikola Tesla Award.

Dan M. Ionel (Fellow, IEEE) is Professor of Electrical Engineering and the L. Stanley Pigman Chair in Power with the University of Kentucky, Lexington, KY, USA, where he is also the Director of the Power and Energy Institute of Kentucky and of the SPARK Laboratory. Previously, he held positions in industry, most recently as Chief Engineer with Regal Beloit Corporation, Grafton, WI, USA, and before that as Chief Scientist with Vestas Wind Turbines. He was also a Visiting Professor and a Research Professor with the University of Wisconsin and Marquette University, Milwaukee, WI. Currently, he is also a Leverhulme Visiting Professor expanding collaborations in England with University of Bath and University of Oxford.

He received the M.Eng. and Ph.D. degrees in electrical engineering from the Polytechnic University of Bucharest, Bucharest, Romania, where his doctoral program included a Leverhulme Visiting Fellowship with the University of Bath, Bath, U.K. He was a Postdoctoral Researcher with the SPEED Laboratory, University of Glasgow, Glasgow, U.K.

Dr. Ionel has contributed to technology developments with long lasting industrial impact, designed electric machines and drives with ratings between 0.002 and 10,000hp, holds more than 40 patents, and has authored or coauthored two books and more than 300 technical papers, including IEEE award winners. He was the recipient of the Cyril G. Veinott Award from the IEEE Power and Energy Society (PES).

He was the Inaugural Chair of the IEEE Industry Applications Society Renewable and Sustainable Energy Conversion Systems Committee, Editor of IEEE Transactions on Sustainable Energy, and Editor-in-Chief of the Electric Power Components and Systems Journal. Dr. Ionel was the Chair of the IEEE PES Electric Motor Subcommittee, the General Chair of the IEEE 2017 Anniversary Edition of the International Conference on Electrical Machines and Drives (IEMDC), and Chair of the IEEE IEMDC Steering Committee.